

NASA/TM-2019-220293



Electromagnetic Modeling for the Conformal Lightweight
Antenna System for Aeronautical Communications
Technologies (CLAS-ACT) Program: Final Report

Anne I. Mackenzie
Langley Research Center, Hampton, Virginia

July 2019

NASA STI Program . . . in Profile

Since its founding, NASA has been dedicated to the advancement of aeronautics and space science. The NASA scientific and technical information (STI) program plays a key part in helping NASA maintain this important role.

The NASA STI program operates under the auspices of the Agency Chief Information Officer. It collects, organizes, provides for archiving, and disseminates NASA's STI. The NASA STI program provides access to the NTRS Registered and its public interface, the NASA Technical Reports Server, thus providing one of the largest collections of aeronautical and space science STI in the world. Results are published in both non-NASA channels and by NASA in the NASA STI Report Series, which includes the following report types:

- **TECHNICAL PUBLICATION.** Reports of completed research or a major significant phase of research that present the results of NASA Programs and include extensive data or theoretical analysis. Includes compilations of significant scientific and technical data and information deemed to be of continuing reference value. NASA counter-part of peer-reviewed formal professional papers but has less stringent limitations on manuscript length and extent of graphic presentations.
- **TECHNICAL MEMORANDUM.** Scientific and technical findings that are preliminary or of specialized interest, e.g., quick release reports, working papers, and bibliographies that contain minimal annotation. Does not contain extensive analysis.
- **CONTRACTOR REPORT.** Scientific and technical findings by NASA-sponsored contractors and grantees.

- **CONFERENCE PUBLICATION.** Collected papers from scientific and technical conferences, symposia, seminars, or other meetings sponsored or co-sponsored by NASA.
- **SPECIAL PUBLICATION.** Scientific, technical, or historical information from NASA programs, projects, and missions, often concerned with subjects having substantial public interest.
- **TECHNICAL TRANSLATION.** English-language translations of foreign scientific and technical material pertinent to NASA's mission.

Specialized services also include organizing and publishing research results, distributing specialized research announcements and feeds, providing information desk and personal search support, and enabling data exchange services.

For more information about the NASA STI program, see the following:

- Access the NASA STI program home page at <http://www.sti.nasa.gov>
- E-mail your question to help@sti.nasa.gov
- Phone the NASA STI Information Desk at 757-864-9658
- Write to:
NASA STI Information Desk
Mail Stop 148
NASA Langley Research Center
Hampton, VA 23681-2199

NASA/TM-2019-220293



Electromagnetic Modeling for the Conformal Lightweight Antenna System for Aeronautical Communications Technologies (CLAS-ACT) Program: Final Report

Anne I. Mackenzie
Langley Research Center, Hampton, Virginia

National Aeronautics and
Space Administration

Langley Research Center
Hampton, Virginia 23681-2199

July 2019

The use of trademarks or names of manufacturers in this report is for accurate reporting and does not constitute an official endorsement, either expressed or implied, of such products or manufacturers by the National Aeronautics and Space Administration.

Available from:

NASA STI Program / Mail Stop 148
NASA Langley Research Center
Hampton, VA 23681-2199
Fax: 757-864-6500

Contents

Abstract.....	1
I. Experiment Purpose.....	1
II. Software and Computers.....	1
III. Methods.....	2
A. Element Models.....	2
1. Cavity-backed patch element in Antenna Magus.....	2
2. Circular patch designed in Antenna.Magus.....	2
3. Stacked patch designed at GRC.....	2
B. Array Models.....	2
1. Linear arrays, flat and curved.....	2
2. Three-dimensional arrays, flat and curved.....	3
3. Windowing and phased array steering.....	3
a. Sidelobe Reduction.....	3
b. Pointing.....	3
C. Equivalent Sources.....	4
1. Near field calculated for one element, multiple copies arranged into an array.....	4
2. Near field measured for array on the T-34C.....	4
D. Airplane Platform Models.....	4
1. Hemicylinder.....	4
2. Closed Cylinder.....	4
3. Ikhana.....	5
4. Global Hawk.....	5
5. T-34C.....	5
E. Solver Methods.....	6
IV. Example Results.....	6
A. Total Radiation Pattern in Two Planes for a 49x49 Array with Radius of Curvature 24 Inches... ..	6
B. Effect of Pointing Angle in a 49x49 Array.....	7
C. Effect of Curvature on Grating Lobes in a 49x49 Array.....	8
D. Effect of Element Spacing on Grating Lobes in a 49x49 Array.....	9
E. Scaling 9x9 to 49x49 Element Array Characteristics.....	9
F. A Possible Antenna Array Design Technique: Change Pointing Direction by Illuminating Different Sections of a Large Array.....	10
G. Sidelobe Nulling.....	10
H. Simulations with Hemicylinder.....	11
I. Simulations with Cylinder.....	11
J. Simulations with Simplified Global Hawk Body Section.....	12
K. Simulations with Global Hawk Forward Section and Radome.....	13
L. Simulations with the T-34C.....	14
V. Publications.....	15

Figures

Figure1. Circular patch used for initial simulations before the final experimental stacked layer patch had been designed.....	2
Figure 2 (a) Array layout for 50x50 patches on a curved surface of radius 16 in. (b) Far field pattern for a 50x50 planar array of circular patches. 3-dB beamwidth = 1.8°.....	3
Figure 3. A hemisphere over a single patch showing where near field data were calculated.....	4
Figure 4. Arrangement of near field points to represent a 9x9 array on a perfect electrical conductor	

(PEC) half cylinder.....	4
Figure 5. Model of the Ikhana with a PEC hemicylindrical antenna platform in the antenna compartment area.....	5
Figure 6. Model of the Global Hawk including the forward portion, radome, antenna platform, and wings.....	5
Figure 7. Model of the T-34C.....	5
Figure 8. 49x49-element rectangular array, radius of curvature = 24 in., 0.3 pedestal cosine window, element spacing = 0.6λ	6
Figure 9. Signal magnitude window is 0.3 pedestal cosine.....	6
Figure 10. Gain pattern in x-z plane where surface is curved, cavity-backed patch elements. 1 st sidelobe level = 22.8 dB.....	6
Figure 11. Gain pattern in y-z plane where surface is not curved, cavity-backed patch elements.....	6
Figure 12. Total far-field gain, x-z plane, 0.55λ spacing in x-y plane, 49x49 array of cavity-backed patch elements pointing at $\theta = 5, 10, \text{ or } 20^\circ$, 16-inch radius of curvature, 45 dB Taylor window.....	7
Figure 13. Gain patterns in x-z plane for radius of curvature = (a) 8 in., (b) 16 in., (c) 24 in., 49x49 array with cosine window, 0.6λ element spacing, cavity-backed patch elements.....	8
Figure 14. Gain patterns in x-z plane for element spacing = $0.65, 0.60, \text{ and } 0.55 \lambda$, 49x49 array with cosine window, 16-inch radius of curvature, cavity-backed patch elements. Wider spacing increases the grating lobe height.....	9
Figure 15. Total far-field x-z gain at $\phi = 180^\circ$, 9x9 or 49x49 array.....	9
Figure 16. With 92 total elements and 49 elements illuminated at one time, the scanning extent is $\pm 42.7^\circ$. Here the left (a) or right side (b) is shown illuminated. The element spacing is 0.6λ or 1.78° , the radius of curvature, 16 in.....	10
Figure 17. Layout for an 8x8 triangular array with 0.3 cosine taper. Radius of curvature = 16 in.....	10
Figure 18. x-z radiation pattern for an array of cavity-backed patches as shown in figure 17. By sidelobe nulling, a notch is produced at 30° elevation.....	10
Figure 19. 8x8 triangular lattice, circular patch near fields as sources, 0.3 cosine window, located at $\theta = 45^\circ$ on a PEC hemicylinder of radius 16 in., length = 32 in.....	11
Figure 20. 3-D radiation pattern calculated for the 8x8 array on a hemicylinder, MLFMM.....	11
Figure 21. 8x8-element rectangular array layout, 0.3 cosine taper.....	11
Figure 22. Circular patch near fields are shown as sources for the 8x8 array on a PEC closed cylinder of radius 16 in. and length 32 in.....	11
Figure 23. 2-D radiation patterns in two planes for the 8x8 array on a closed PEC cylinder, MLFMM..	11
Figure 24. Near fields for 8x8 triangular array of stacked circular patches on a PEC hemicylindrical platform mounted close to the left side of a Global Hawk body section.....	12
Figure 25. Total far field in two planes calculated for the 8x8 array on a section of the Global Hawk, PO solution. The theta' phi' coordinate system puts $\theta' = 0^\circ$ at $\theta = 45^\circ$	12
Figure 26. Near fields for 8x8 triangular array of stacked circular patches on a PEC hemicylindrical platform mounted close to the right side of a section of a Global Hawk with radome.....	13
Figure 27. Total far field in two planes calculated for the 8x8 array on a section of the Global Hawk with radome, PO solution. The theta' phi' coordinate system puts $\theta' = 0^\circ$ at $\theta = 45^\circ$	13
Figure 28. T-34C with (a) calculated near field data for 8x8 array elements and (b) measured OEWG data for the array on the airplane.....	14
Figure 29. Magnitude and phase information for the 8x8 phased array, which is designed to point 30° up from horizontal.....	14
Figure 30. 3-D total radiation pattern using the calculated element near fields, PO solution.....	14
Figure 31. Polar plot of total far field gain at $\phi = 178^\circ$ for the two simulation methods, PO solution...	15

Tables

Table 1. Gain Values, Taylor Weighting.....	7
Table 2. Gain Values at Pointing Angle = 0° , $\Phi = 180^\circ$	9

Abstract

A series of electromagnetic simulations was conducted for the Conformal Lightweight Antenna System for Aeronautical Communications Technologies (CLAS-ACT) Program. The program designed, built, and flight tested a 14.25 GHz conformal patch array antenna for satellite communications on a T-34C airplane. Various studies were performed to evaluate the effects of antenna element spacing, array shape, signal taper, phased array pointing angle, null steering coefficients, antenna platform, and location on the airplane. This report documents the methods and some of the results of tests done over a 2 ½ year period.

I. Experiment Purpose

The Conformal Lightweight Antenna System for Aeronautical Communications Technologies (CLAS-ACT) Program was conducted between 2017 and 2019 and funded by the Convergent Aeronautics Solutions (CAS) portion of the NASA Aeronautics Research Mission Directorate. The purpose of the experiment was to develop a conformal array antenna making use of the lightweight Aero-Zero substrate materials invented at Glenn Research Center (GRC). The antenna was to operate at 14.25 GHz and be flown on a UAV to allow satellite communication with the airplane, a capability which in turn would allow beyond line-of-sight command and control. Furthermore, the phased array antenna radiation pattern was to be characterized by a notch such that transmissions from the airplane towards the ground would not interfere with ground instruments operating at the same frequency. During the antenna development, computational models were used to simulate the antenna patterns resulting from the use of various antenna designs, on and off the airplane. 3-D radiation patterns were supplied to team members at Ames Research Center (AMC) to incorporate into their Systems Tool Kit (STK) software to aid with experiment flight planning. This report describes the electromagnetic modeling performed for the CLAS-ACT program. Given that over 60 reports were submitted on this subject to the Principal Investigators, Drs. Mary Ann Meador and Jim Downey, this paper summarizes only some of the methods and results.

II. Software and Computers

MATLAB was used to create array layout files and to assemble data into the formats required by the various commercial software products in use. Portable Batch System script files were written to provide instructions to work problems on the Langley Research Center (LaRC) K-Cluster computers. Antenna Magus was used to design simple patches, to display array layouts, and to calculate field patterns for patch antennas and array designs. Simulations of an array mounted on an airplane were calculated in ALTAIR FEKO to produce far field files, which were the desired outputs. PREFEKO files, which have their own scripting language, mesh files generated from drawings in CADFEKO, and near field files generated from FEKO models all became inputs for FEKO simulations. Airplane models were downloaded from share sites such as GrabCAD and 3dcadbrowser.com.

Smaller problems were calculated on an HP Z840 workstation, while larger problems were sent to the Langley K-Cluster. Some of the problems became quite large, as the airplanes were on the order of 521 wavelengths (Ikhana) or 416 wavelengths (T-34C).

III. Methods

A. Element Models

1. *Cavity-backed patch element in Antenna Magus*

Initially, it was desired to calculate the effect of patch antenna spacing, array shape, phase inputs for antenna pointing, and window functions for sidelobe reduction. However the patch antenna itself had not been designed. A number of simulations were performed using the far field for an ideal cavity-backed patch as the source. This method was implemented in Antenna Magus software and simply added far fields together, therefore neglecting mutual impedance effects.

2. *Circular patch designed in Antenna Magus*

Later, a simple circular patch antenna as shown in figure 1 was designed and its near field or far field was used as the source for array simulations.

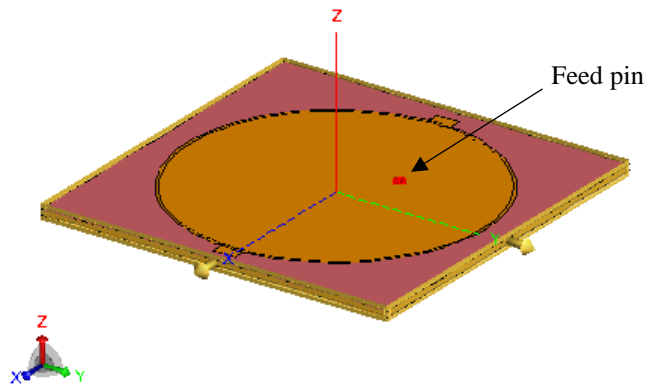


Figure 1. Circular patch used for initial simulations before the final experimental stacked layer patch had been designed.

3. *Stacked patch designed at GRC*

Still later, team members at Glenn Research Center (GRC) designed a multilayer stacked patch antenna and calculated near field data for that patch, which became the source for array simulations. In simulations containing the mounting platform or part or all of an airplane, the use of near fields as radiation sources allowed the computational problem to be performed on a computer which could not have accommodated the individual design geometry for all of the array elements in addition to the airplane. Near field data were provided as calculated in a spherical or hemispherical shape around the patch.

B. Array models

1. *Linear arrays, flat and curved*

Some relatively simple simulations used a flat or curved single line of elements.

2. Three-dimensional arrays, flat and curved

Three-dimensional simulations included 8x8, 9x9, 49x49, or 50x50 elements. It was calculated that at least 50x50 elements would be needed to achieve the desired 2-degree beam width. Because the array size would be 2^n and to simplify the initial antenna construction, an 8x8 antenna was fabricated for flight testing. Therefore many of the simulations incorporated the array size 8x8. Figure 2 shows an example of (a) the array layout for a 50x50 curved array and (b) the field pattern for a 50x50 planar array.

Originally, a hemicylindrical antenna platform was designed to mount the antenna inside the antenna compartment of the Ikhana. It was intended that this shape would simulate the curved surface of an airplane on which an array antenna might be mounted. The hemicylinder was chosen to have a radius of 16 inches; therefore a number of simulations incorporated the 16-inch radius into the shape of the array curve. Later, the airplane was changed to a Global Hawk, and still later, due to scheduling problems, a T-34C (Navy trainer) on which a flat antenna array was mounted on the left side of the airplane.

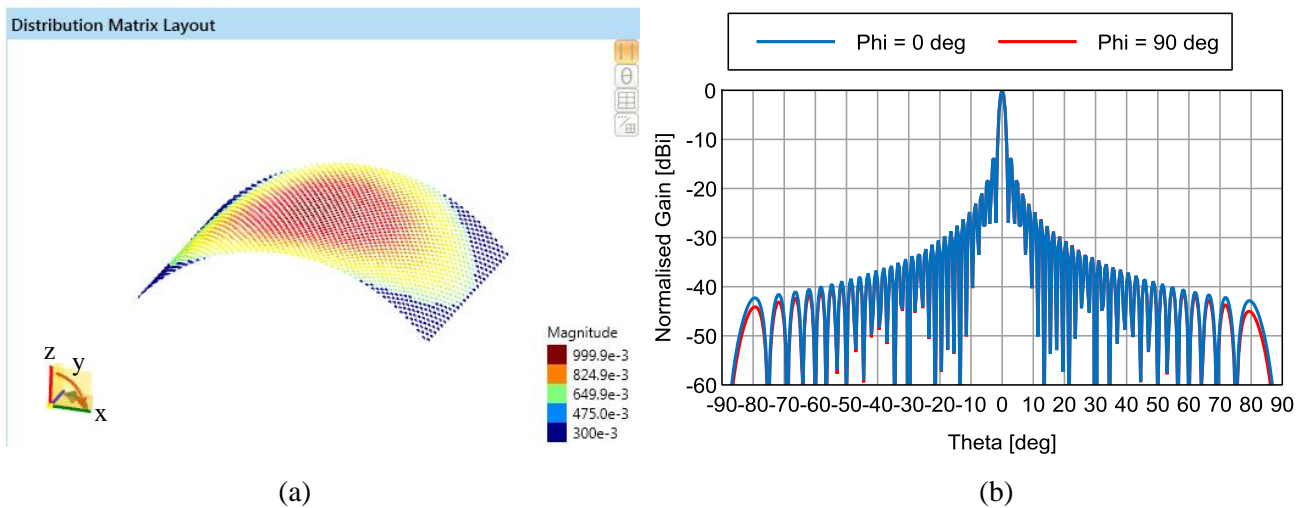


Figure 2 (a) Array layout for 50x50 patches on a curved surface of radius 16 in. (b) Far field pattern for a 50x50 planar array of circular patches. 3-dB beamwidth = 1.8°.

3. Windowing and phased array steering

a. Sidelobe Reduction

Sidelobe reduction was accomplished through the use of various window functions; the window most commonly employed being a 0.3 pedestal cosine taper applied to the signal magnitudes. Figure 2 (a) shows 2500 elements in an array for which the signal magnitude taper is indicated by the color scale.

b. Pointing

Beam pointing was accomplished by varying the signal phase across the array. GRC personnel calculated a series of complex coefficients to apply to signals at the 8x8 flight array feed points to produce null steering, that is, a radiation notch at a particular angle where it was desired to prevent interference with instruments on the ground.

C. Equivalent Sources

1. Near field calculated for one element, multiple copies arranged into an array

Given that each patch element had a complex structure which would be too computationally intensive to model 2500 or even 64 times, the computational load was lessened by using near field data as radiation sources when computing array radiation patterns. Near electric and magnetic fields were calculated for a single element at a radius of 100 mm from the patch center, and multiple copies of the near field data hemisphere were arranged in a geometrical pattern corresponding to the array layout spacing and angular orientation. Figures 3 and 4 show, respectively, such a hemisphere and 81 groups of hemispherically arranged near field data points. Some simulations were also performed with near fields calculated in a spherical pattern around each patch element.

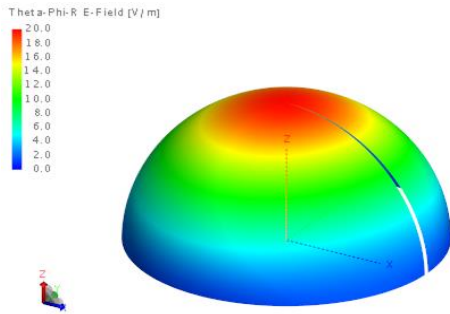


Figure 3. A hemisphere over a single patch showing where near field data were calculated.

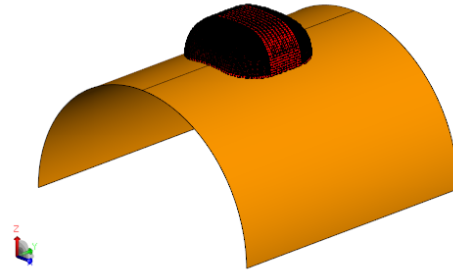


Figure 4. Arrangement of near field points to represent a 9x9 array on a perfect electrical conductor (PEC) half cylinder.

2. Near field measured for array on the T-34C

When available, measured near field data for the entire array on the airplane were used as an equivalent source. GRC personnel provided near field data measured at GRC and at Armstrong, both data sets based on the 8x8 array antenna mounted on a T-34C. By means of an open-ended waveguide (OEWG), the near field was measured in a vertically oriented rectangle approximately 4.5 inches from the side of the airplane; data were collected at 1862 (38x49) points or 2622 (46x57) points.

D. Airplane Platform Models

1. Hemicylinder

When the experiment began, the designated aircraft was the NASA Ikhana and the intended location for the antenna array was inside the Ikhana's antenna compartment under a radome. The usual antenna gimbals assembly was to be removed and in its place there would be a hemicylindrical platform on which the phased array would be mounted. Following this plan, many simulations were performed with an array drawn in a hemicylindrical shape. Figure 4 shows one example of a half cylinder built into the simulation and used as the antenna platform.

2. Closed cylinder

Some simulations were performed with an array mounted on a large reflective closed cylinder, in the absence of an airplane model.

3. *Ikhana*

A good computer aided drawing (CAD) of the Ikhana, shown in figure 5, was obtained from the US Army; however it was not used in simulations because of the large size making it impractical to run on available computers even with the multilevel fast multipole method (MLFMM), an efficient but fairly accurate approximation method.

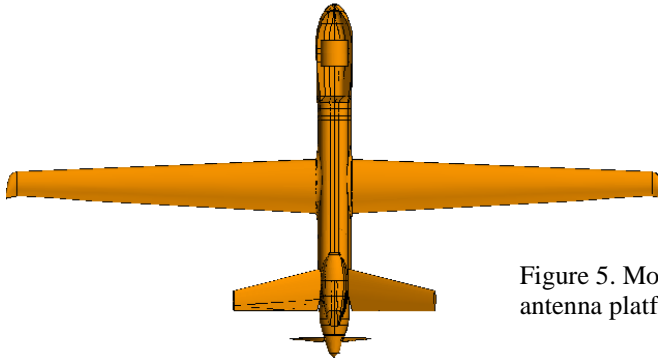


Figure 5. Model of the Ikhana with a PEC hemicylindrical antenna platform in the antenna compartment area.

4. *Global Hawk*

A drawing of the Global Hawk was obtained from GrabCAD and a portion of this model was used together with the physical optics (PO) simulation method for some simulations. Figure 6 shows a portion of the Global Hawk including the radome, hemicylindrical antenna platform, and wings.

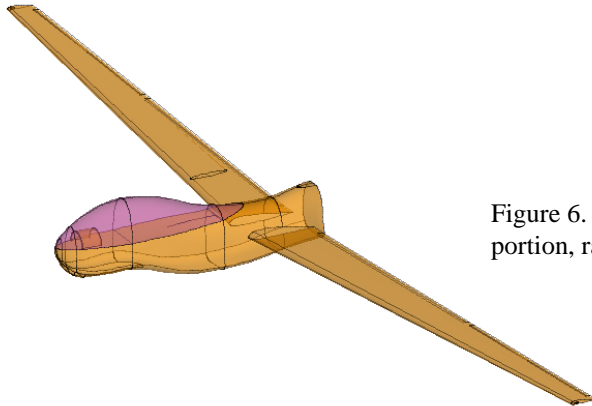


Figure 6. Model of the Global Hawk including the forward portion, radome, antenna platform, and wings.

5. *T-34C*

A drawing of a T-34C was obtained from 3dcadbrowser.com for simulations using the PO method. These simulations ran on the K-Cluster in about 7 hours. The model is shown in figure 7.

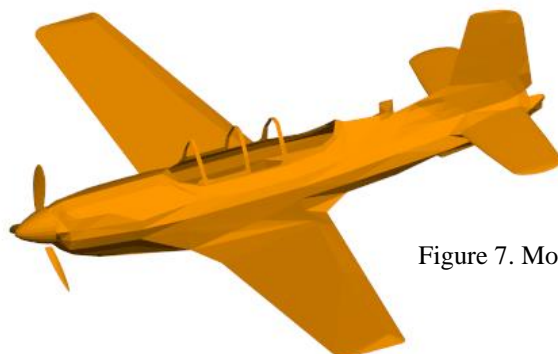


Figure 7. Model of the T-34C.

E. Solver methods

The method of moments (MOM) is a full wave solver method which is very accurate. MLFMM and PO are approximate electromagnetic simulation methods which produce slightly less accurate results but require much less computer memory and time for solutions.

IV. Example Results

A. Total Radiation Pattern in Two Planes for a 49x49 Array, Radius of Curvature 24 In.

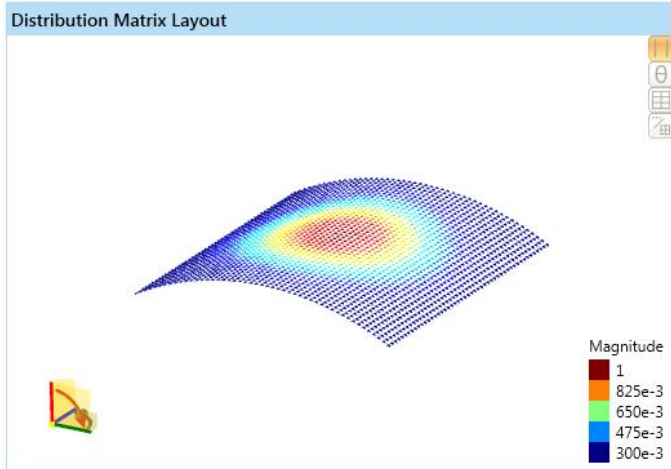


Figure 8. 49x49-element rectangular array, radius of curvature = 24 in., 0.3 pedestal cosine window, element spacing = 0.6λ .

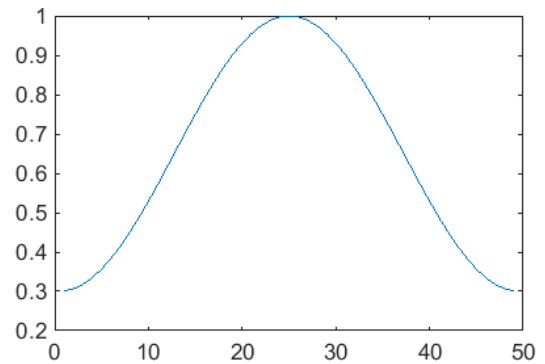


Figure 9. Signal magnitude window is 0.3 pedestal cosine.

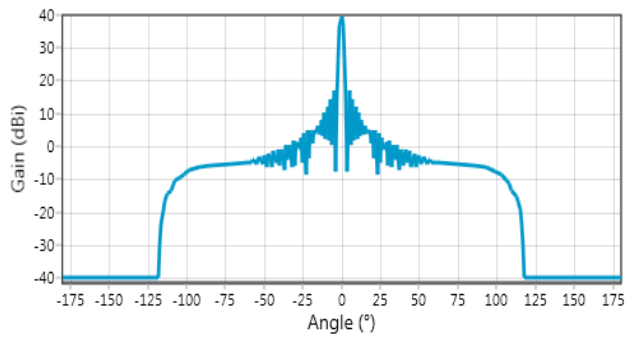


Figure 10. Gain pattern in x-z plane where surface is curved, cavity-backed patch elements. 1st sidelobe level = 22.8 dB.

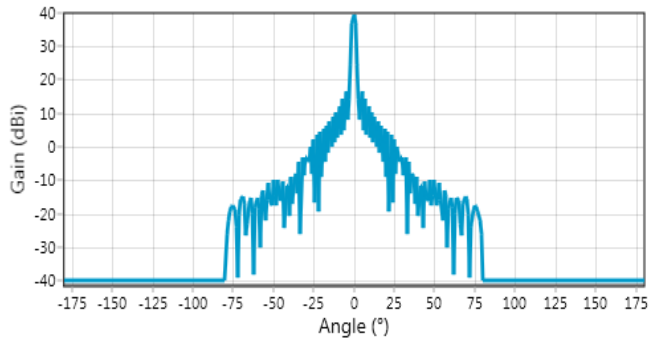


Figure 11. Gain pattern in y-z plane where surface is not curved, cavity-backed patch elements.

For a cylindrically curved surface as shown in figure 8, the far field radiation pattern looks quite different in the two principal vertical planes, as shown in figures 10 and 11. This simulation incorporated a 49x49-element array with a 0.3 cosine window applied. The cosine window is shown by the color scale in figure 8 and is graphed in figure 9.

B. Effect of Pointing Angle in a 49x49 Array

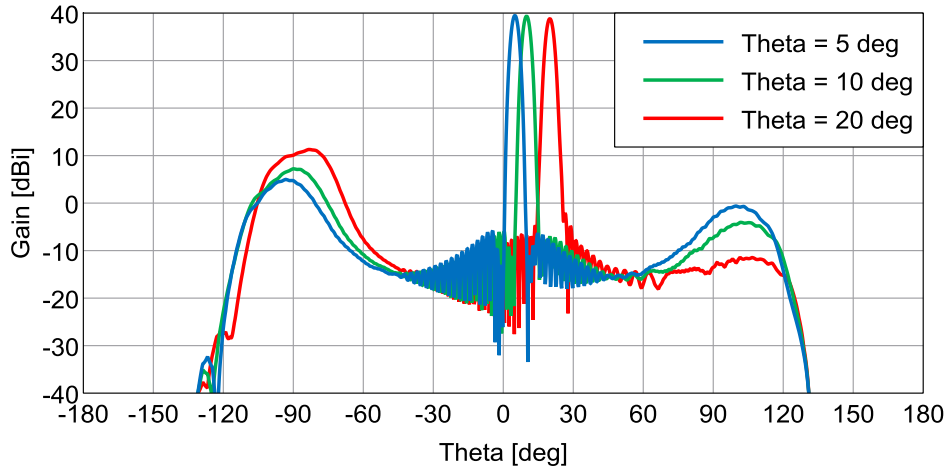


Figure 12. Total far-field gain, x-z plane, 0.55λ spacing in x-y plane, 49x49 array of cavity-backed patch elements pointing at $\theta = 5, 10,$ or 20° , 16-inch radius of curvature, 45 dB Taylor window.

Table 1. Gain Values, Taylor Weighting

Pointing Angle Theta [deg] at Phi = 180°	Peak Gain [dBi]	3-dB Beamwidth [deg]	1 st Sidelobe Level [dB]	Grating Lobe Level [dB]
5.0	39.5	2.9	-50.5	-34.5
10.0	39.4	2.9	-48.0	-32.1
20.0	38.8	3.1	-40.9	-27.5

As the pointing angle deviates farther from zenith, gain is decreased, beamwidth increased, and grating lobes vary depending on which side of the main beam they are on.

C. Effect of Curvature on Grating Lobes in a 49x49 Array

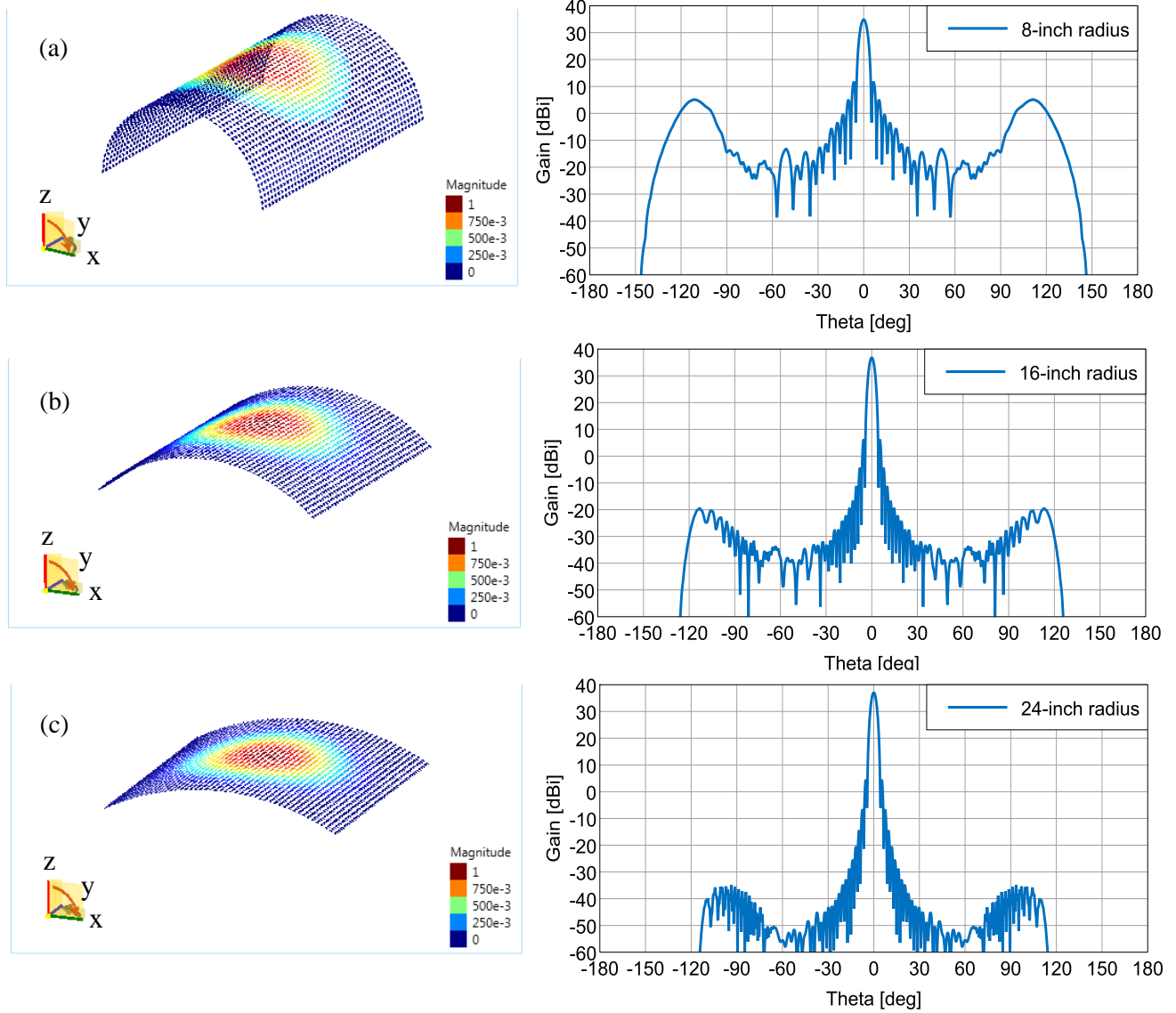


Figure 13. Gain patterns in x-z plane for radius of curvature = (a) 8 in., (b) 16 in., (c) 24 in., 49x49 array with cosine window, 0.6λ element spacing, cavity-backed patch elements.

Grating lobes are seen to decrease in height with lesser surface curvature, as shown in figure 13.

D. Effect of Element Spacing on Grating Lobes in a 49x49 Array

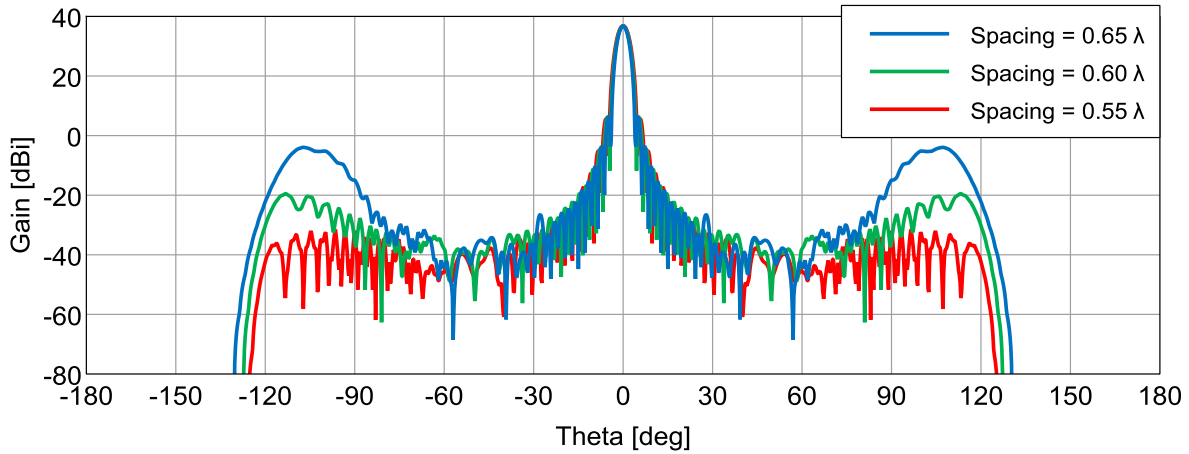


Figure 14. Gain patterns in x-z plane for element spacing = 0.65, 0.60, and 0.55 λ , 49x49 array with cosine window, 16-inch radius of curvature, cavity-backed patch elements. Wider spacing increases the grating lobe height.

E. Scaling 9x9 to 49x49 Element Array Characteristics

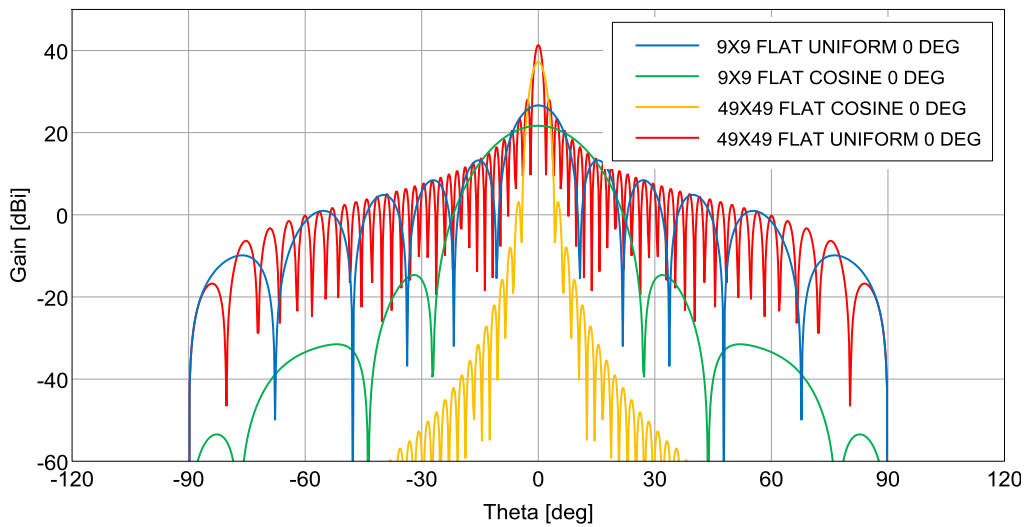


Figure 15. Total far-field x-z gain at $\phi = 180^\circ$, 9x9 or 49x49 array.

Table 2. Gain Values at Pointing Angle $\Theta = 0^\circ$, $\Phi = 180^\circ$

	9x9 elements	49x49 elements	Difference [dB]	Note: Sidelobe level is the difference between the peak gain and the 1 st sidelobe gain.
Peak value, uniform [dBi]	26.6	41.4	14.7	
Peak value, cosine [dBi]	21.7	37.3	15.6	
1 st sidelobe level, uniform [dB]	13.4	13.3	-0.1	
1 st sidelobe level, cosine [dB]	36.3	34.0	-2.3	
1 st sidelobe level, cosine improvement over uniform [dB]	23.0	20.8	-2.2	

In a uniform, planar array, the peak power is proportional to the number of elements. The first sidelobe level varies according to the window function applied to the element feeds.

F. A Possible Antenna Array Design Technique: Change Pointing Direction by Illuminating Different Sections of a Large Array

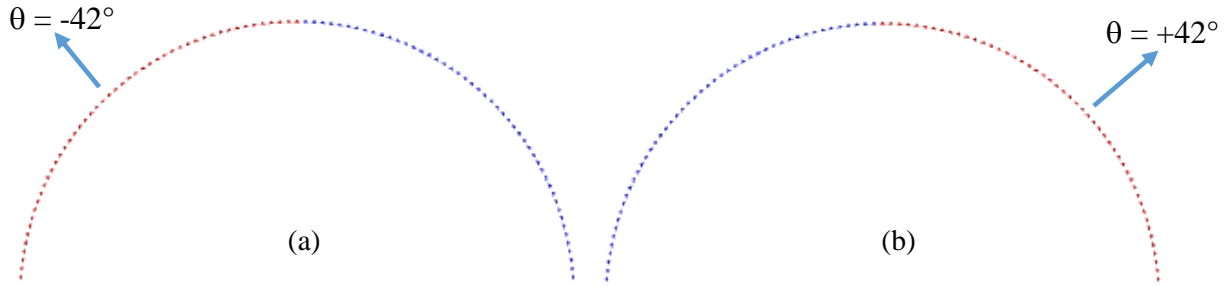


Figure 16. With 92 total elements and 49 elements illuminated at one time, the scanning extent is $\pm 42.7^\circ$. Here the left (a) or right side (b) is shown illuminated. The element spacing is 0.6λ or 1.78° , the radius of curvature, 16 in.

G. Sidelobe Nulling

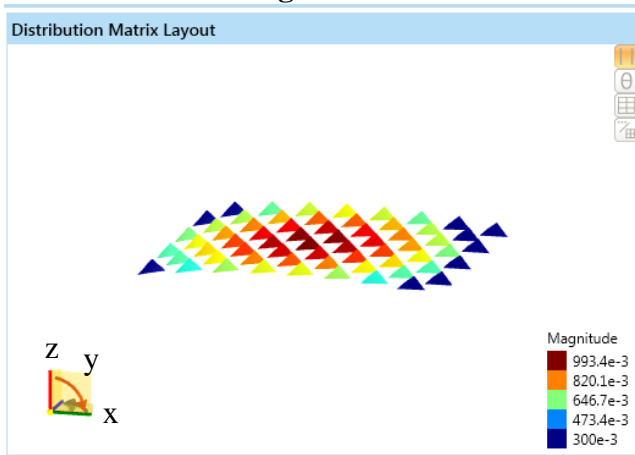


Figure 17. Layout for an 8x8 triangular array with 0.3 cosine taper. Radius of curvature = 16 in.



Figure 18. x-z radiation pattern for an array of cavity-backed patch elements as shown in figure 17. By sidelobe nulling, a notch is produced at 30° elevation .

By controlling the complex signal coefficients, a narrow null can be created in the radiation pattern at a desired angle, in this case, 30° elevation.

H. Simulations with Hemicylinder

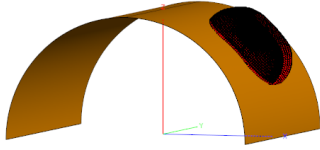


Figure 19. 8x8 triangular lattice, circular patch near fields as sources, 0.3 cosine window, located at $\theta = 45^\circ$ on a PEC hemicylinder of radius 16 in., length = 32 in.

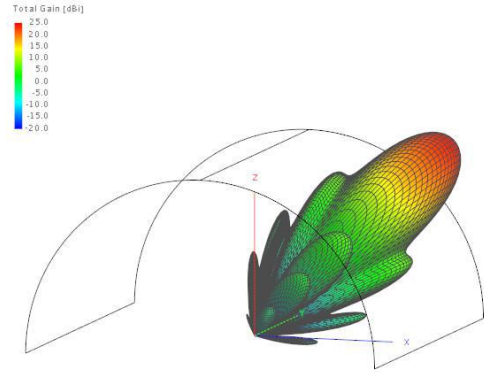


Figure 20. 3-D radiation pattern calculated for the 8x8 array on a hemicylinder, MLFMM.

I. Simulations with Cylinder

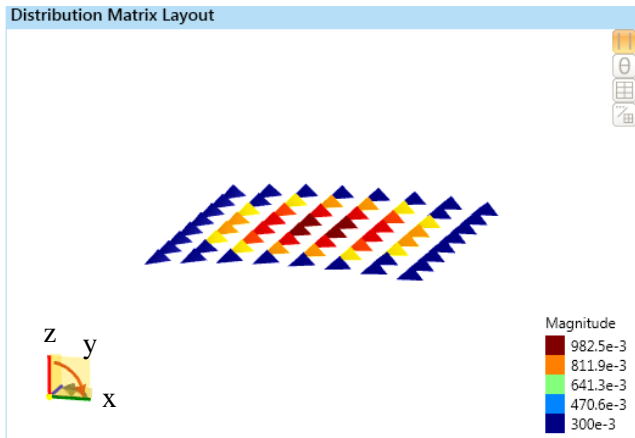


Figure 21. 8x8-element rectangular array layout, 0.3 cosine taper.

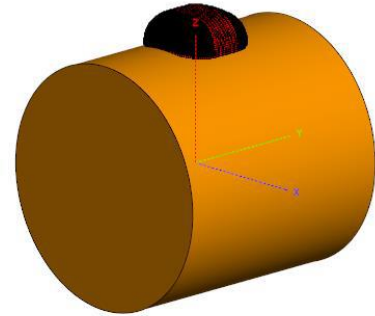


Figure 22. Circular patch near fields are shown as sources for the 8x8 array on a PEC closed cylinder of radius 16 in. and length 32 in.

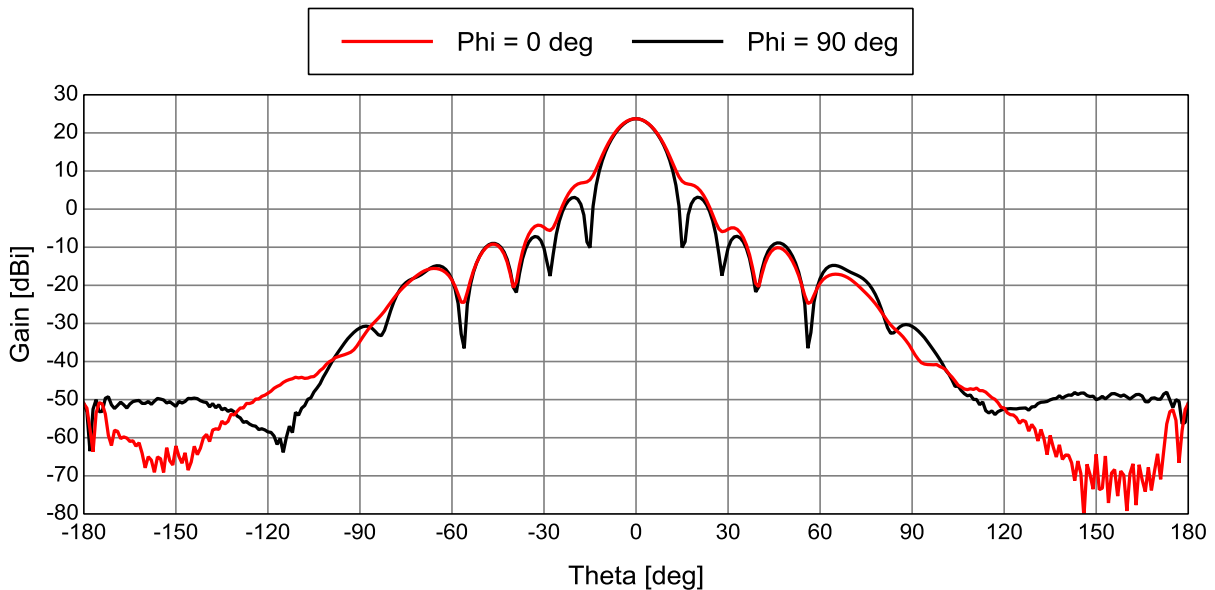


Figure 23. 2-D radiation patterns in two planes for the 8x8 array on a closed PEC cylinder, MLFMM.

J. Simulations with Simplified Global Hawk Body Section

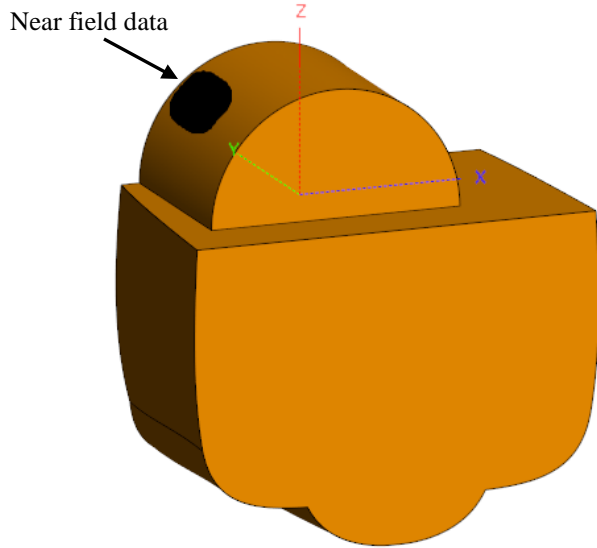


Figure 24. Near fields for 8x8 triangular array of stacked circular patches on a PEC hemicylindrical platform mounted close to the left side of a Global Hawk body section.

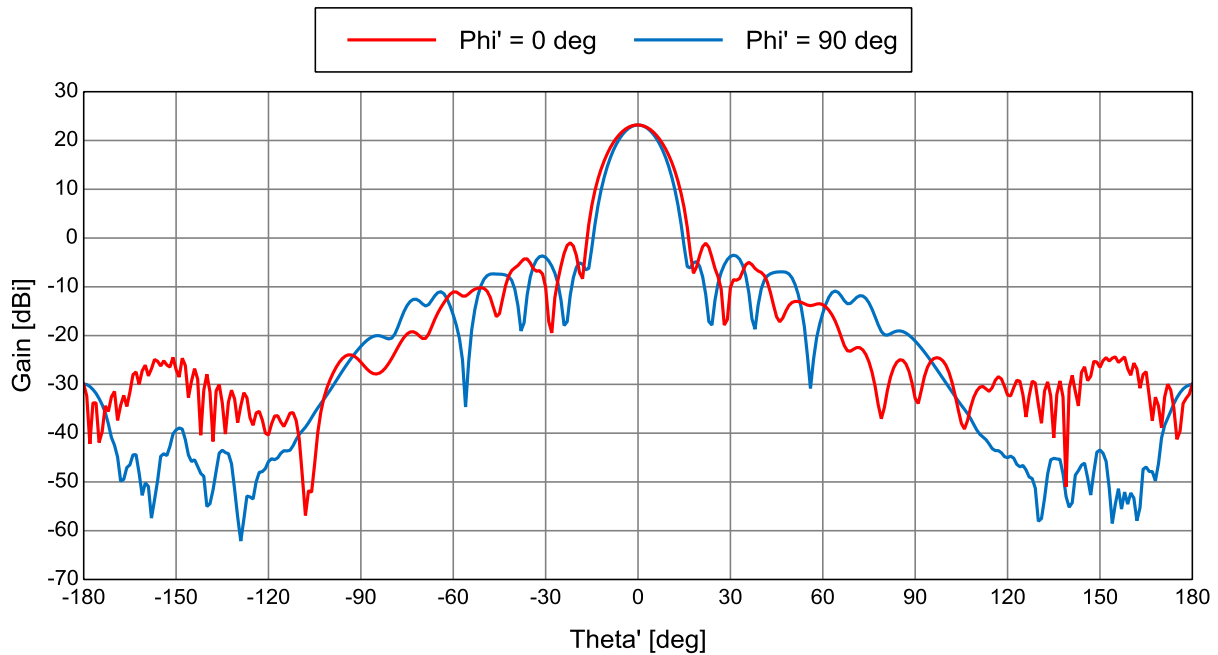


Figure 25. Total far field in two planes calculated for the 8x8 array on a section of the Global Hawk, PO solution. The theta' phi' coordinate system puts $\theta' = 0^\circ$ at $\theta = 45^\circ$.

In order to approximate the shape of a very large airplane, a section of the body was approximated and used as a model.

K. Simulations with Global Hawk Forward Section and Radome

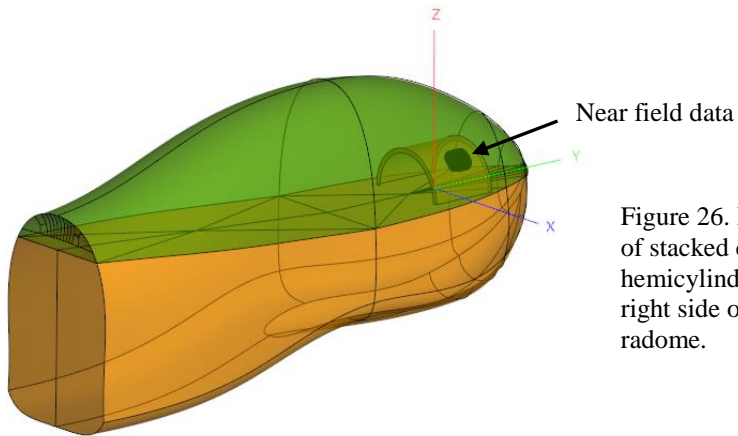


Figure 26. Near fields for 8x8 triangular array of stacked circular patches on a PEC hemicylindrical platform mounted close to the right side of a section of a Global Hawk with radome.

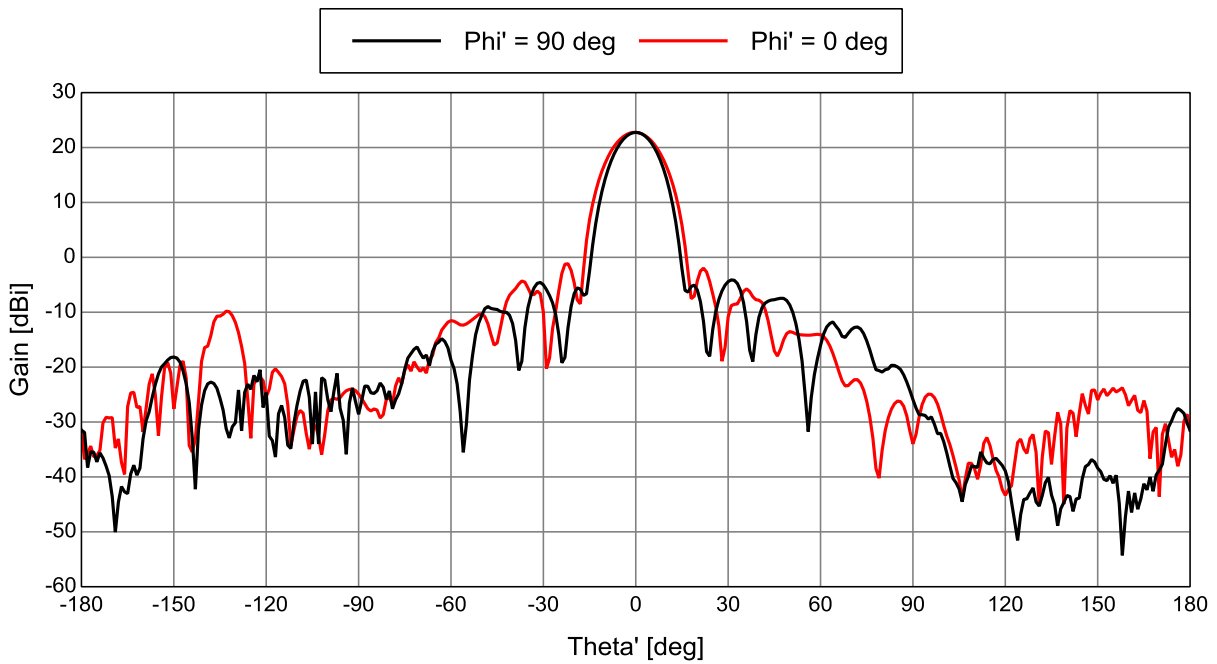


Figure 27. Total far field in two planes calculated for the 8x8 array on a section of the Global Hawk with radome, PO solution. The theta' phi' coordinate system puts $\theta' = 0^\circ$ at $\theta = 45^\circ$.

L. Simulations with the T-34C

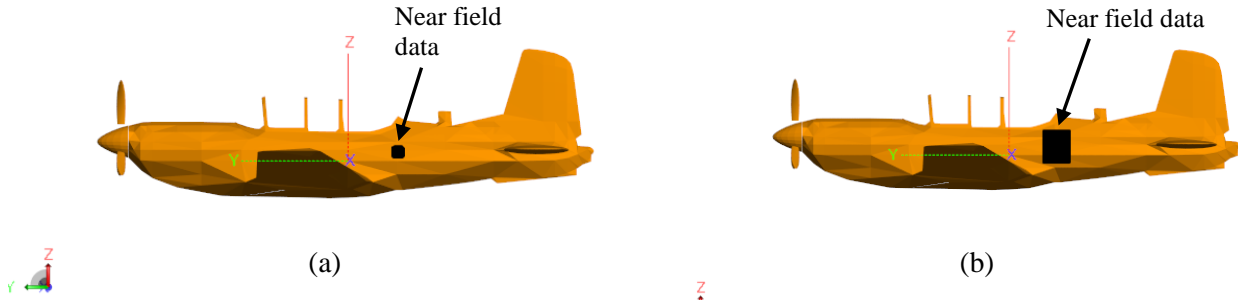


Figure 28. T-34C with (a) calculated near field data for 8x8 array elements and (b) measured OEWG data for the array on the airplane.

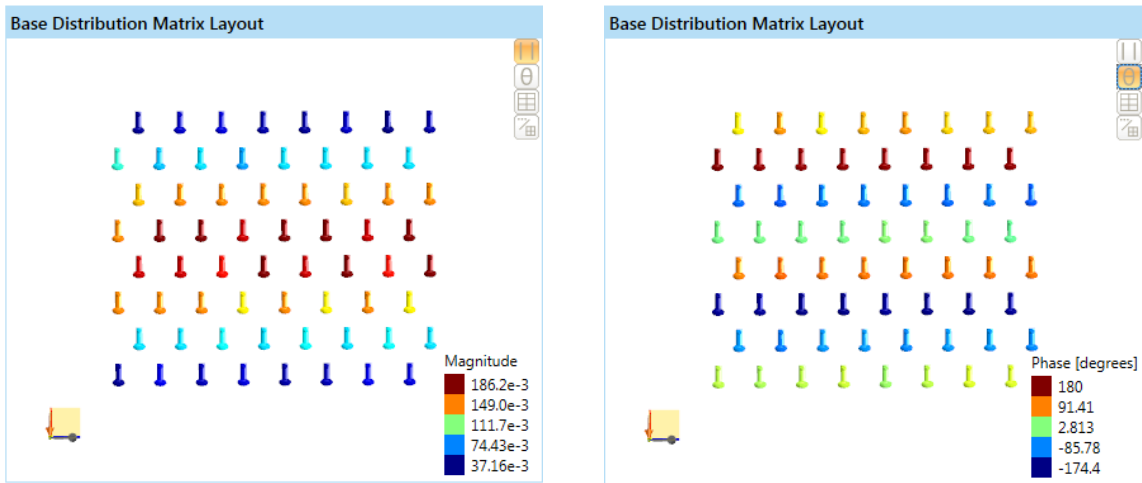


Figure 29. Magnitude and phase information for the 8x8 phased array, which is designed to point 30° up from horizontal.

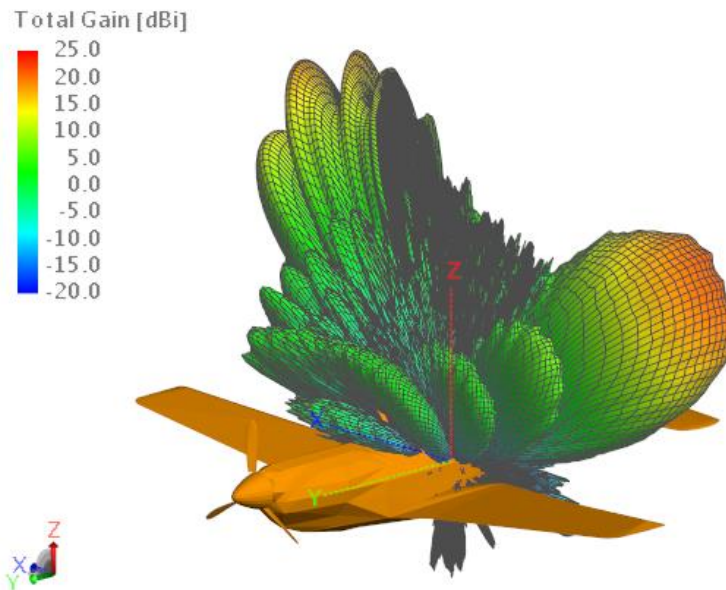


Figure 30. 3-D total radiation pattern using the calculated element near fields, PO solution.

Figure 28 shows the locations of two types of near field data that were used as sources for simulations with the T34-C airplane model. In figure 28 (a), the near field data were calculated from the stacked patch model; in figure 28 (b), OEWG near field data were measured while the antenna was radiating and affixed to the side of the airplane. Figure 29 shows the array signal coefficients, magnitude and phase. A 3-D pattern was calculated using each method. Figure 30 shows the 3-D result assuming the calculated element near fields. The maximum gain is seen here to be about 20.1 dBi and the main beam, on the left side, is pointing upward about 30° from the horizon.

Figure 31 shows polar plots of both simulated results at $\phi = 178^\circ$. In the “calculated element near fields” plot, a deep null is seen at -10° elevation. Given the disparity between the results, there is a problem with at least one of the simulations, possibly indicating an incorrect airplane model. The simulation using the element near fields as sources (in blue) is more like the expected pattern with lowered radiation towards the ground.

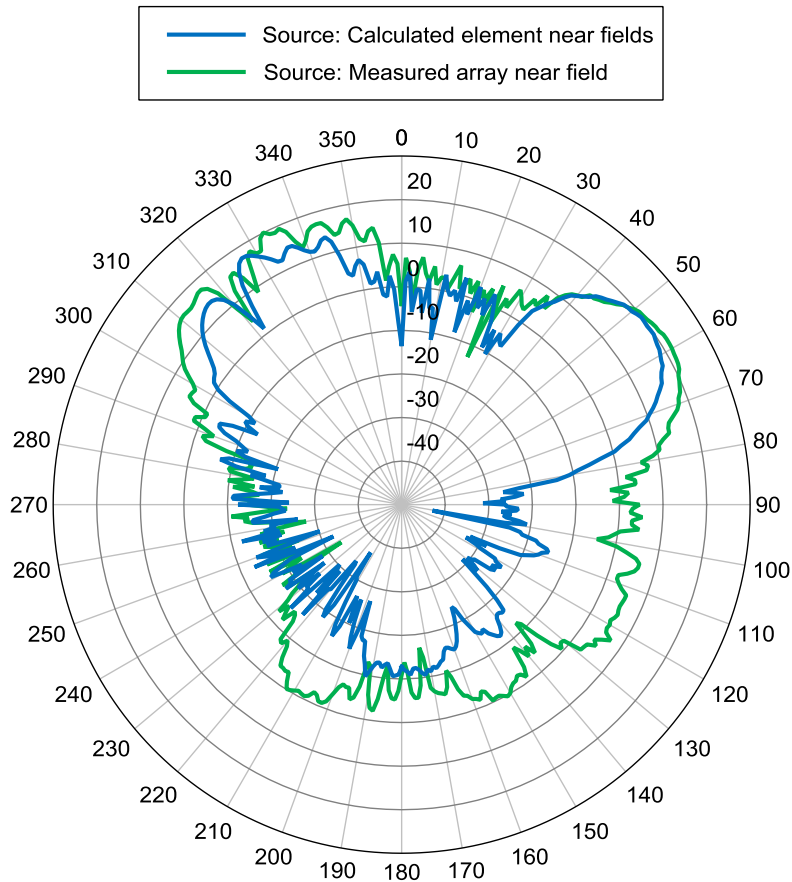


Figure 31. Polar plot of total far field gain at $\phi = 178^\circ$ for two simulation methods, PO solution.

V. Publications

Mackenzie, A.I., Downey, J.M., and Schoenholz, B.L., “Progress on Modeling a Cylindrical Patch Antenna Array for a UAV,” Presentation at the Spring 2017 Advanced Helicopter Electromagnetics Program Review, Fort Eustis, VA, June 20, 2017.

Mackenzie, A.I., “Estimating a Large Phased Array Antenna Radiation Pattern by Computer Electromagnetic Simulation,” NASA/TM-2018-220094, October 2018.

REPORT DOCUMENTATION PAGE

Form Approved
OMB No. 0704-0188

The public reporting burden for this collection of information is estimated to average 1 hour per response, including the time for reviewing instructions, searching existing data sources, gathering and maintaining the data needed, and completing and reviewing the collection of information. Send comments regarding this burden estimate or any other aspect of this collection of information, including suggestions for reducing the burden, to Department of Defense, Washington Headquarters Services, Directorate for Information Operations and Reports (0704-0188), 1215 Jefferson Davis Highway, Suite 1204, Arlington, VA 22202-4302. Respondents should be aware that notwithstanding any other provision of law, no person shall be subject to any penalty for failing to comply with a collection of information if it does not display a currently valid OMB control number.
PLEASE DO NOT RETURN YOUR FORM TO THE ABOVE ADDRESS.

1. REPORT DATE (DD-MM-YYYY) 07/01/2019		2. REPORT TYPE Technical Memorandum		3. DATES COVERED (From - To) October 2016 - June 2019	
4. TITLE AND SUBTITLE Electromagnetic Modeling for the Conformal Lightweight Antenna System for Aeronautical Communications Technologies (CLAS-ACT) Program: Final Report				5a. CONTRACT NUMBER	
				5b. GRANT NUMBER	
				5c. PROGRAM ELEMENT NUMBER	
6. AUTHOR(S) Mackenzie, Anne I.				5d. PROJECT NUMBER	
				5e. TASK NUMBER	
				5f. WORK UNIT NUMBER 533127.02.17.07.05	
7. PERFORMING ORGANIZATION NAME(S) AND ADDRESS(ES) Electromagnetics & Sensors Branch NASA Langley Research Center Hampton, VA 23681-0001				8. PERFORMING ORGANIZATION REPORT NUMBER L-21041	
9. SPONSORING/MONITORING AGENCY NAME(S) AND ADDRESS(ES) National Aeronautics and Space Administration Washington, DC 20546-0001				10. SPONSOR/MONITOR'S ACRONYM(S) NASA	
				11. SPONSOR/MONITOR'S REPORT NUMBER(S) NASA/TM-2019-220293	
12. DISTRIBUTION/AVAILABILITY STATEMENT Unclassified - Unlimited Subject Category 33: Electronics and Electrical Engineering Availability: NASA STI Program (757) 864-9658					
13. SUPPLEMENTARY NOTES					
14. ABSTRACT A series of electromagnetic simulations was conducted for the Conformal Lightweight Antenna System for Aeronautical Communications Technologies (CLAS-ACT) Program. The program designed, built, and flight tested a 14.25 GHz conformal patch array antenna for satellite communications on a T-34C airplane. Various studies were performed to evaluate the effects of antenna element spacing, array shape, signal taper, phased array pointing angle, null steering coefficients, antenna platform, and location on the airplane. This report documents the methods and some of the results of tests done over a 2 ½ year period.					
15. SUBJECT TERMS conformal antenna, electromagnetic modeling, radiation patterns, computational electromagnetics, phased array, satellite communications					
16. SECURITY CLASSIFICATION OF:			17. LIMITATION OF ABSTRACT	18. NUMBER OF PAGES	19a. NAME OF RESPONSIBLE PERSON
a. REPORT	b. ABSTRACT	c. THIS PAGE			STI Help Desk (email: help@sti.nasa.gov)
U	U	U	UU	23	19b. TELEPHONE NUMBER (Include area code) (757) 864-9658